Journal of Alloys and Compounds 696 (2017) 856–868

Contents lists available at ScienceDirect

Journal of Alloys and Compounds

journal homepage: http://www.elsevier.com/locate/jalcom

Electrical and thermomechanical properties of CVI- Si_3N_4 porous rice husk ash infiltrated by Al-Mg-Si alloys

N. Soltani [a, c, *], S. Soltani [b], A. Bahrami [c], M.I. Pech-Canul [a], L.A. Gonzalez [a], A. Möller [d], J. Tapp [d], A. Gurlo [e]

[a] Centro de Investigación y de Estudios Avanzados del IPN Unidad Saltillo, Ave. Industria Metalúrgica No. 1062, Parque Industrial Saltillo-Ramos Arizpe, Ramos Arizpe, Coahuila, 25900, Mexico
[b] Faculty of Electrical and Computer Engineering, K. N. Toosi University of Technology, Tehran 16314, Iran
[c] Instituto de Investigaciones en Materiales, Universidad Nacional Autónoma de México, Ciudad Universitaria, 04510 D.F., Mexico
[d] Institute for Inorganic and Analytical Chemistry, Johannes Gutenberg-University Mainz, Duesbergweg 10-14, 55128 Mainz, Germany
[e] Fachgebiet Keramische Werkstoffe/Chair of Advanced Ceramic Materials, Institut für Werkstoffwissenschaften und −technologien, Technische Universitaet Berlin, Hardenbergstraße 40, 10623 Berlin, Germany

ARTICLE INFO

Article history:
Received 11 November 2016
Received in revised form
2 December 2016
Accepted 3 December 2016
Available online 6 December 2016

Keywords:
Pressureless infiltration
Rice husk ash
Electrical resistivity
Coefficient of thermal expansion
Thermal diffusivity

ABSTRACT

The effect of following processing parameters on the electrical and thermomechanical properties of Al/Si_3N_4 deposited silica composites was investigated using the Taguchi method and analysis of variance (ANOVA): infiltration temperature and time, atmosphere, effect of Si_3N_4 coating, porosity content in the preforms, and magnesium content in the alloy. The contributions of each of the parameters to modulus of elasticity, electrical resistivity, coefficient of thermal expansion (CTE), and thermal diffusivity of the resulting composites were determined. The maximum modulus of elasticity and electrical resistivity of obtained composites were 265 GPa, and 1.37 $\times$ 10^{-3} Ω m, respectively. These values were achieved in composites fabricated from Si_3N_4 preforms under conditions of temperature (1200 °C), time (120 min), porosity of 40 vol %, Al-9Mg-13Si alloy, in the atmosphere of N_2. The minimum value of CTE obtained was 5.3 $\times$ 10^{-6}/°C. This value was achieved in composites fabricated from Si_3N_4 coated silica under the same mentioned conditions. The thermal diffusivity of four fabricated samples (two samples with the highest and two samples with lowest electrical resistivity) was measured. The results show that the highest value of thermal diffusivity (20.4 mm^2/s) among fabricated composites is belonged to the one with highest value of electrical resistivity.

1. Introduction

Particulate reinforced aluminum matrix composites (AMC) have attracted considerable attention in at least the last 25 years because of their potential to exhibit enhanced mechanical and thermal properties in comparison to the individual constituents, both at room temperature and at relatively high temperatures. Nonetheless, their massive production at a cost-effective scale has been hindered by several factors, in addition to the high cost of the manufacturing equipment. Despite the numerous investigations devoted to optimize processing parameters, it is evident that in order to achieve their full potential, more focused investigations have still to be conducted [1–8]. In metal matrix composites by increasing the level of reinforcement the liquid infiltration into porous ceramic preforms is required. For avoiding the need for large pressure the affinity between the metal/ceramic couple in terms of wettability should be increased [9]. Several reinforcing materials have been considered for Al matrix composites, including synthetic (SiC, Si_3N_4, B_4C, Mg_2Si etc.), recycling (fly ash) and natural (rice husk ash (RHA)) materials [10]. Compared to the first two types of reinforcement, the use of RHA is not still widely spread [11–14]. Nonetheless, there are several windows of opportunity for this abundant material [15]. As for its morphology, it has the appearance of flakes with short fibers, which makes it a potential

* Corresponding author. Centro de Investigación y de Estudios Avanzados del IPN Unidad Saltillo, Ave. Industria Metalúrgica No. 1062, Parque Industrial Saltillo-Ramos Arizpe, Ramos Arizpe, Coahuila, 25900, Mexico.
E-mail addresses: niloofar.soltani@cinvestav.mx, nilufar.soltani@gmail.com (N. Soltani).

http://dx.doi.org/10.1016/j.jallcom.2016.12.051
0925-8388/

candidate for improving strength [16,17]. For the most part, it is composed by silicon dioxide (SiO_2), which as it is generally accepted, as an oxide, it restricts the wettability of RHA by liquid Al. As with other reinforcement materials prone to dissolution or deleterious reactions, one potential approach for preventing sabotage the properties of RHA, is the use of coatings which improve wetting, protect the reinforcement from attack by liquid Al or enhance the matrix/reinforcement interface strength. From the various techniques for the preparation of films/coatings, chemical vapor deposition and infiltration (CVD/CVI) is one that properly allows the coating of particles/fibers prior to the preparation of the MMC. Moreover, the hybrid system chemical vapor deposition and infiltration (HYSYCVD and HYSYCVI) recently developed offers a number of advantages compared with the traditional CVD and CVI techniques [18]. Sequential infiltrations processes could be proposed to the preparation of AMC reinforced with RHA, the first in gas phase for coating of RHA, and the second, with the metal in liquid state to fabricate AMC.

The aim of this investigation was concerned on understanding the phenomena associated to the preparation of composites by infiltration method and accomplishing systematic study in order to optimize the processing parameters affecting on microstructure, physical and mechanical properties.

2. Experimental procedure

2.1. Pressureless infiltration process

Si_3N_4 was deposited onto silica porous preforms via HYSY-CVI (hybrid precursor system chemical vapor infiltration) method, using N_2-NH_3 gas mixture at flow rate of 100 cm^3/min and Na_2SiF_6 compact powder as gaseous and solid precursors, respectively, at 1300 °C for 90 min. Infiltration of porous Si_3N_4 powder and Si_3N_4 deposited into RHA preform by Al-Mg-Si alloys were conducted under the conditions shown in Table 1. Infiltration temperature, time, coating, type of atmosphere, porosity of preform and Mg content in Al alloy were used as parameters of infiltration process. Each of these parameters was tested at two levels. Accordingly, those that were found out to have a considerable effect on the properties are included. Furthermore, these parameters were considered both in the interaction between time and temperature and in the interaction between alloy and atmosphere.

Infiltration trials were performed in alumina tube closed at both ends with end-cap fittings to control the process atmosphere. The mold-preform-metal assembly was placed in the center of the alumina tube and heated at the test temperature. The chamber was held in an isothermal state for various test times in defined atmosphere for each test temperature. Finally, the cooling process to room temperature was carried out in the absence of gas and the system was cooled in the controlled atmosphere down to ~550 °C. Table 2 shows L16 Taguchi tables used for this study.

Table 1
Parameters and levels tested in the experiment for system of Si_3N_4 coated silica and Si_3N_4.

Parameters	Level 1	Level 2
Temp.	900 °C	1200 °C
Time	60 min	120 min
Atmosphere	N_2	Ar
Porosity	40	60
Coating	Si_3N_4 coated silica	Si_3N_4
Alloy	Alloy 1 (Low Mg)	Alloy 2 (High Mg)
Interaction 1	Temperature × Time	
Interaction 2	Alloy × atmosphere	
Constants	Gas flow rate of N_2 and Ar: 20 cm^3/min, Heating and cooling rate = 20 °C/min, amount of alloy: 20gr	

2.2. Characterization of fabricated composites

Three-dimensional Xray computer tomography was used for characterization of macroscopic porosity of RHA preform before and after HYSYCVI. Then the volume was visualized by VGStudio MAX 2.2. The X-ray powder diffraction (XRD) tests were performed using Philips −3040 XRD equipment (Cu Kα radiation, anode excitation of 40 kV, and current of 30 mA). Microstructure analyses were conducted using scanning electron microscope (SEM) Philips XL30 at an acceleration voltage of 20 KeV. Transmission electron microscopy (TEM) analyses have been done by a conventional TECNAI $G^2$20 S-TWIN from FEI-Company with LaB_6 electron emitter, 200 KV acceleration voltage and 0.24 nm point resolution. Images were acquired by a GATAN MS794 P CCD-Camera with 1024 × 1024 pixels. For elemental analysis, an EDAX Si (Li)-Energy-dispersive X-ray spectroscopy (EDX) r-TEM SUTW Detector was used. The modulus of elasticity of the composite was determined using an ultrasonic technique (ASTM standard E494-95, Standard Practice for Measuring Ultrasonic Velocity in Materials). CTE of the starting materials and all fabricated composites were measured using a thermomechanical analyzer -vertical Dilatometer, TMA 402 F1/F3 Hyperion®. The samples were heated from room temperature up to 300 °C for four cycles with heating and cooling rates of 20 °C/min. Electrical resistivity and conductivity were measured using four-point probe technique (Lucas Labs S-302 Four Point Probe) on the flat surfaces of the samples. For an infinite slice of finite thickness w, one can be express the resistivity as [19]:

$$\rho = \rho_s w = \frac{V}{I} w \frac{\pi}{\ln 2} F\left(\frac{w}{s}\right) \quad (1)$$

where $F(w/s)$ is a correction factor approaching unity as w approaches zero.

The thermal diffusivity values in different temperatures were measured using a Netzsch LFA 457 MicroFlash™ diffusivity apparatus.

Table 2
L16 Taguchi table designed for pressureless infiltration process for system of Si_3N_4 coated silica and Si_3N_4.

Trial/Run	A	B	C	D	E	F	G	H
1	1	1	1	1	1	1	1	1
2	1	1	1	1	1	2	2	2
3	1	1	1	2	2	2	1	1
4	1	1	1	2	2	1	2	2
5	1	2	2	1	1	2	1	2
6	1	2	2	1	1	1	2	1
7	1	2	2	2	2	1	1	2
8	1	2	2	2	2	2	2	1
9	2	1	2	1	2	1	2	1
10	2	1	2	1	2	2	1	2
11	2	1	2	2	1	2	2	1
12	2	1	2	2	1	1	1	2
13	2	2	1	1	2	2	2	2
14	2	2	1	1	2	1	1	1
15	2	2	1	2	1	1	2	2
16	2	2	1	2	1	2	1	1

A: Alloy × Atm.
B: Porosity.
C: Temp. × Time.
D:Alloy.
E: Atmosphere.
F: Si_3N_4 Coating.
G: Time.
H: Temperature.

3. Results and discussions

3.1. Preform preparation

As it can be observed from Fig. 1(a), the preform is crack free and the porosities are distributed uniformly through the preform. Fig. 1(b) illustrate the preform after CVI process. Due to higher density and molecular weight of Si_3N_4, the preform appears in lighter shade in comparison to the preform before CVI process. The bright spots in Fig. 1(b) could be corresponded to the agglomeration of Si_3N_4 fibers in the spaces between RHA particles. No defects in the scale of higher than 5 mm, such as microcracks are found in the inner structure of the preform.

3.2. Phase analysis of fabricated composites

XRD patterns of a number of fabricated composites are presented in Fig. 2. The JCPDS Card Number of phases are: Si_3N_4 (JCPDS Card No. 73-1210), Al (JCPDS Card No. 04-0787), Si (JCPDS Card No. 27-1402), AlN (JCPDS Card No. 75-1620), Si_2N_2O (JCPDS Card No. 83-2142), $MgAl_2O_4$ (JCPDS Card No. 77-0435), MgO (JCPDS Card No: 78-0430) and Mg_2SiO_4 (JCPDS Card No. 71-1081). Depending on the Mg concentration in alloys, atmosphere and material of preform, the presence of different phases such as spinel ($MgAl_2O_4$), magnesium oxide (MgO) and aluminum nitride (AlN) were detected. AlN was detected in all the fabricated composites. Thus, it seems this phase plays a key role in all the physical and mechanical properties of the composites. As it might be seen, the AlN peaks are more intense at higher temperatures and in the presence of nitrogen. Therefore, under these appropriate conditions AlN can be favorably formed. Besides, formation of MgO and $MgAl_2O_4$ were just observed in coated silica preforms. MgO exists in addition to $MgAl_2O_4$ at higher Mg content alloy.

SEM micrographs of the infiltrated Si_3N_4 composites under the condition of L2 is illustrated in Fig. 3. The black, gray and bright regions correspond to the pores, ceramic phase and the Al–Mg-Si alloy, respectively. It can be seen that the preform was completely infiltrated with a homogeneous distribution of ceramic phase. A few fine pores in the composite show a good wetting between ceramic surfaces and molten alloy. Presence of AlN phase in micrograph shows that there exists high chemical reaction between Si_3N_4 and Al-Mg Alloy due to the lack of Si_3N_4 in the micrographs. Considering L1 test condition, abundant of non-infiltrated regions were observed in fabricated composite. This can be attributed to the short time and low temperature of fabrication process that restrict the infiltration of Al through the Si_3N_4 fibers. Under L12 condition, $MgAl_2O_4$ is noticed besides AlN phase that can be due to the reaction of molten alloy with uncoated silica. SEM micrographs of the infiltrated composites by considering the processing parameters of L12 and 15 are shown in Fig. 4. In infiltrated composite (L12) the great level of diffusion of Mg at the primary stage of reaction leads to the formation of MgO needles on the surface of un-coated silica. Thus, the production of the consequent reaction between MgO needles, Al and Mg would be Al-Mg-O, in the form of fine platelets (two-dimension) (L12). The amount of Al/Mg ratio is estimated very low in these fine platelets. The configuration of octahedron of $MgAl_2O_4$ due to the compounding of 8 grown plates, can be easily observed in infiltrated composite (L15). The growth of the platelets can be probably attributed to the adhesion to one another or continuing diffusion of Al and Mg and their reactions with SiO_2. The platelets are oriented at random from the parallel to perpendicular directions with respect to the interface. As the platelet size goes up, the Al concentration enhances and finally it experiences the Al/Mg ratio of 2 [20,21].

TEM micrograph of fabricated composite (Fig. 5) under L12 condition shows that AlN crystals (appearing in black) are homogeneously well-embedded in the Al matrix. No porosity at the matrix–ceramic boundary is observed on this scale. EDX analyses carried out inside the matrix demonstrate the presence of magnesium, silicon and some oxygen. Moreover, they show a substantial increment in the amount of silicon near to the matrix–ceramic interface. $MgAl_2O_4$ crystals also have been detected by EDX analyses.

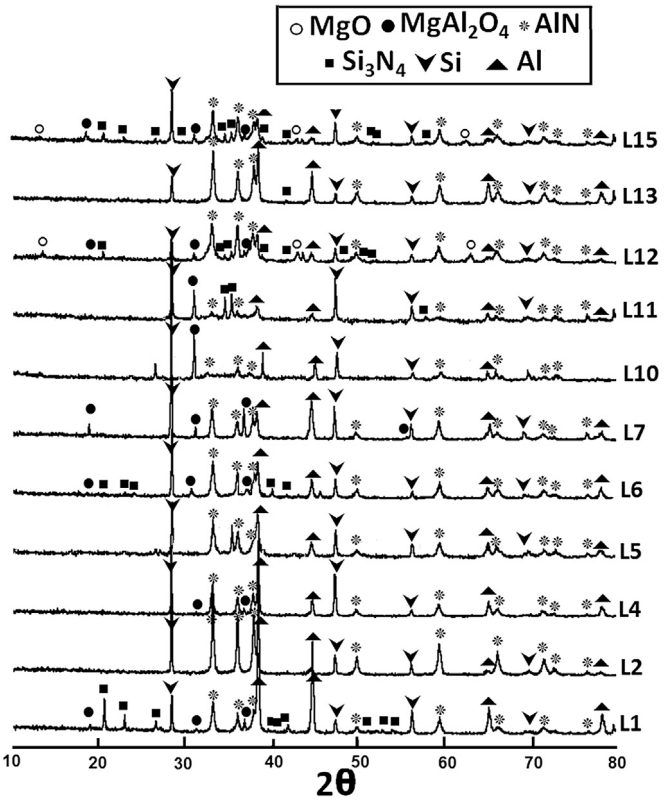

Fig. 2. XRD pattern of infiltrated Si_3N_4 and coated silica composite for all test specimens.

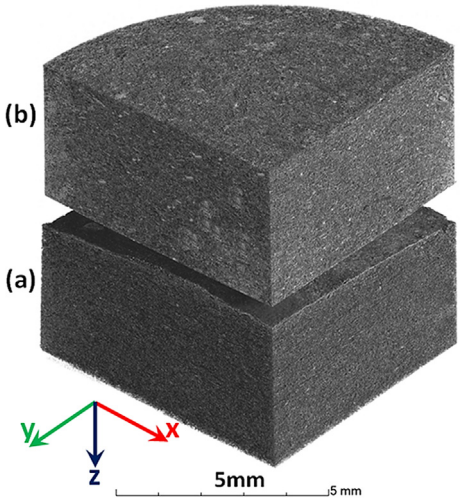

Fig. 1. A 3D tomographic image of RHA preforms, a) before, and b) after CVI process.

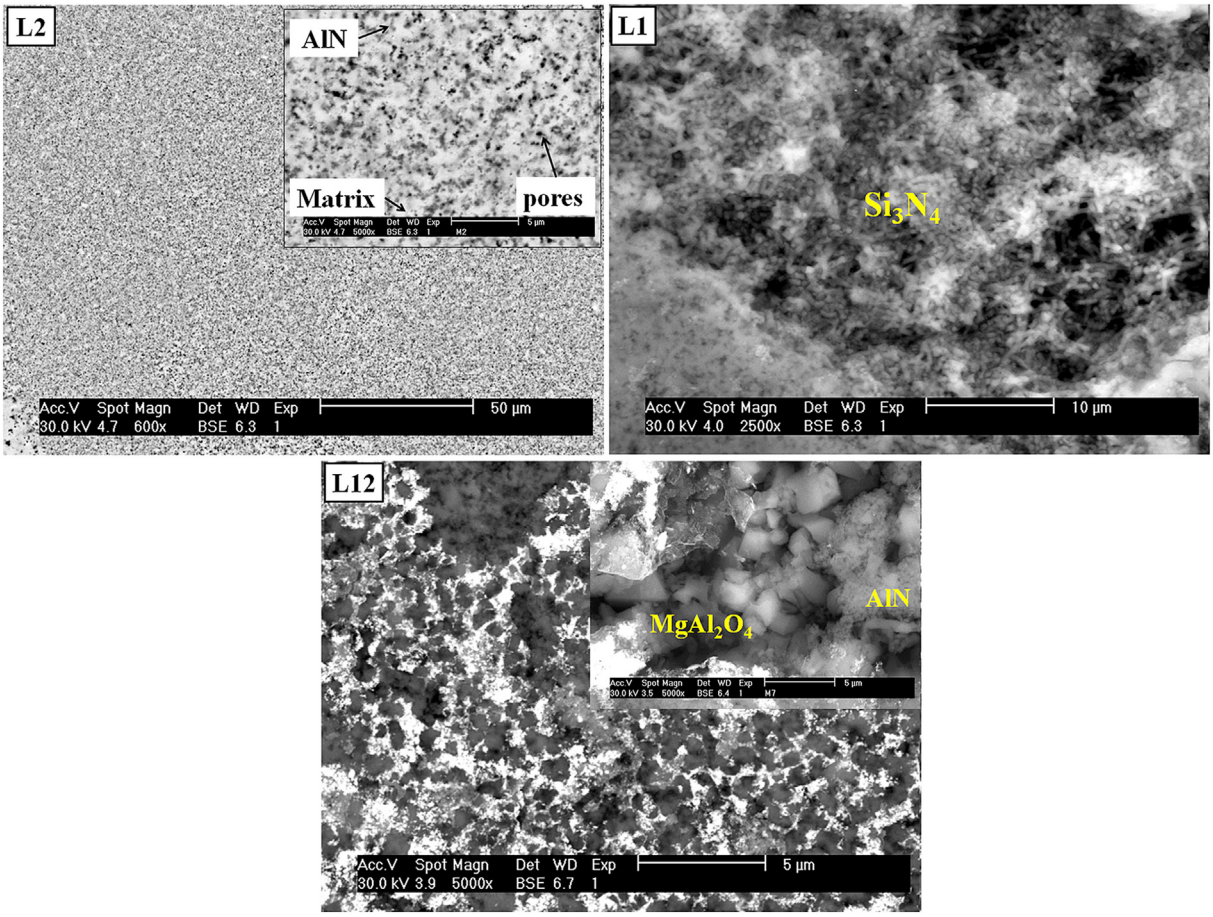

Fig. 3. SEM micrographs of infiltrated composites under condition of L2, L1 and L12.

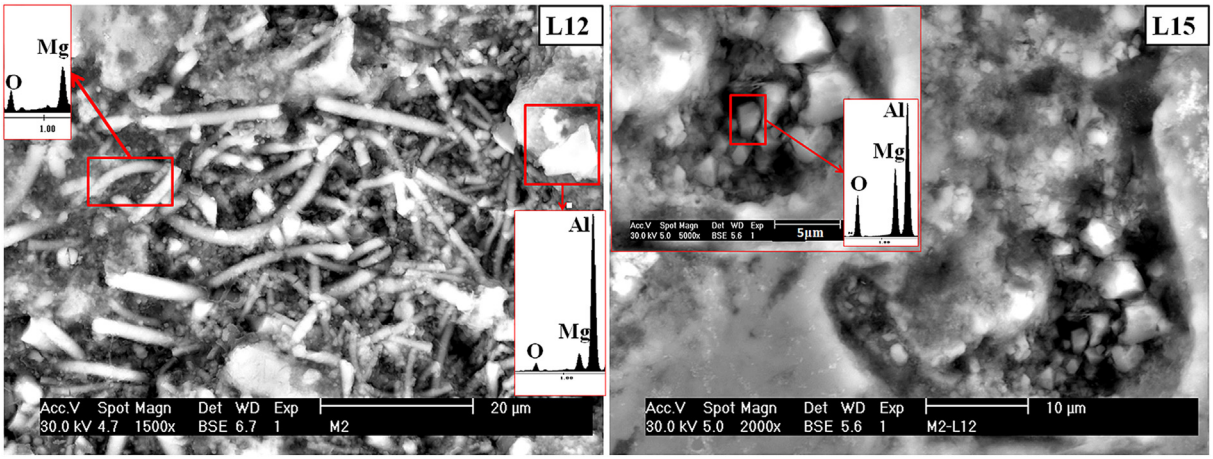

Fig. 4. SEM micrographs of infiltrated composites under condition of L12 and L15.

3.3. Modulus of elasticity

The fundamentals of the method are based on calculating the modulus of elasticity (E) at room temperature from the velocity of an ultrasonic pulse propagating in the composite, which is waveguide sealed to a specimen by means of a couplant. The modulus of elasticity was calculated according to [22]:

$$V_L = \left[\frac{E(1-\nu)}{\rho(1-\nu)(1-2\nu)}\right]^{1/2} \quad (2)$$

$$\nu = \frac{1-2(V_T/V_L)^2}{2-2(V_T/V_L)^2} \quad (3)$$

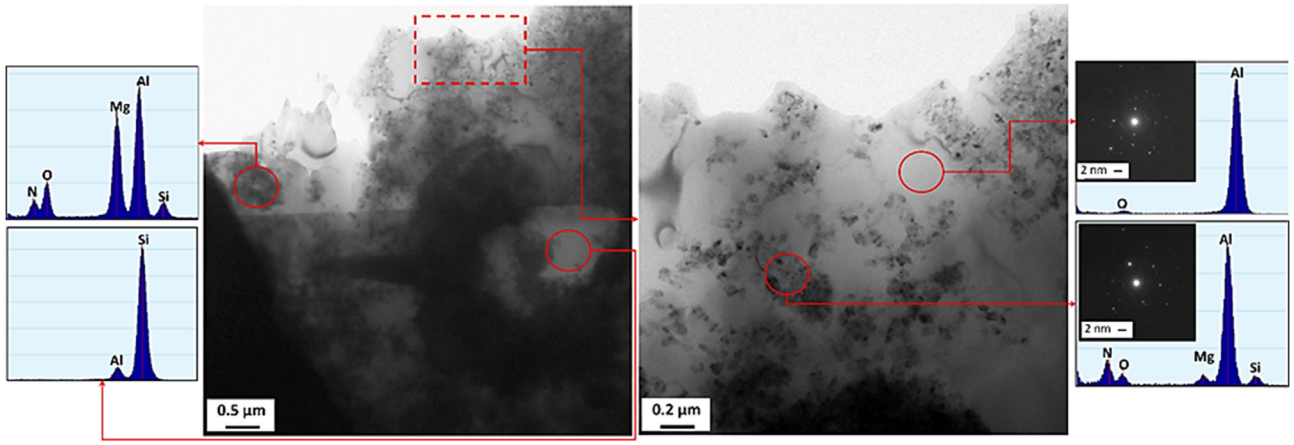

Fig. 5. TEM micrographs and EDS of infiltrated composites under condition of L12.

$$V_T = \frac{V_L}{2} \tag{4}$$

$$E = \frac{(V_L)^2 \rho}{1.499} \tag{5}$$

where E is Young's modulus (GPa), V_L is Longitudinal wave velocity (m/s), V_T is Transverse wave velocity (m/s), ν is Poisson's ratio (dimensionless) and ρ is Density (kg/m^3).

Fig. 6 indicates young's modulus values of fabricated composite. Results of the pooled ANOVA for the modulus of elasticity are shown in Table 3. It implies that, at the studied levels, the parameter that most significantly affects the modulus of elasticity of composites is the process temperature. As can be seen, Its relative contribution to the variance in the modulus of elasticity values is 43%. Expectedly, due to capillary effects, this parameter has a significant contribution to the modulus of elasticity values since, an inadequate temperature may restrict the elevation of the liquid metal. The residual porosity in the composites negatively affects the wave velocity since wave propagation is higher in solids than in air. Atmosphere of infiltration process also has a notable effect on modulus of elasticity of the composite, contributing 31% of the variance. This is probably due to the formation of AlN in the presence of N_2 during the process. The *Temperature* × *Time* interaction, Mg content of the alloy and time also have effects on the E with

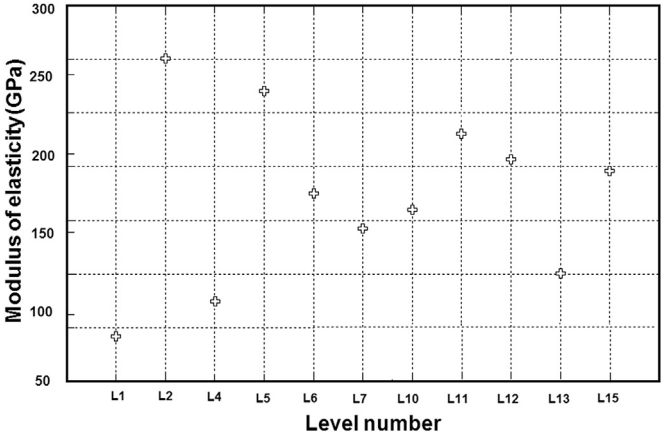

Fig. 6. Young's modulus values of fabricated composite.

Table 3
Pooled ANOVA table for modulus of elasticity (E).

T	Factors	Sum of squares	Variance	Contribution percentage
1	Alloy × Atmosphere	Pooled	Pooled	–
2	Porosity	Pooled	Pooled	–
3	Temperature × Time	9346	9346	7
4	Alloy	2295	2295	2
5	Atmosphere	42580	42580	31
6	Coating	Pooled	Pooled	–
7	Time	3387	3387	3
8	Temperature	58388	58388	43
	Error	19038	6346	14
	Total	135987		100

relative contributions of 7, 2 and 3%, respectively. The percent contribution due to the error term in this analysis is 14%. The percent contribution due to the error term provides a good criterion of the adequacy of the experiment. If the error term is low, i.e., 15% or less, it is assumed that no important factors were omitted from the experiment, and no measurement errors were significant. Considering the parameters included in Table 3, in the ranges tested, the maximum modulus of elasticity can be obtained by using the process parameters shown in Table 4. By using these process parameters, the projected modulus of elasticity is 250 ± 9 GPa, which is in good agreement with the verification value of 265 GPa.

3.4. Electrical resistivity and conductivity

Fig. 7 shows those values for pure Al, alloy 1 and alloy 2. It depicts that alloying with Mg and Si cause a reduction in electrical conductivity of pure Al. Reduced conductivity in solid solutions is explained as follows. Atoms of two related metals with defined similarity incorporate side by side into the same crystal lattice to

Table 4
Optimal process parameters for maximum modulus of elasticity.

Parameters	Proposed levels
Temperature (°C)	1200
Time (min)	120
Porosity (%)	40
Alloy	Low Mg
Atmosphere	N_2
Substrate	Si_3N_4

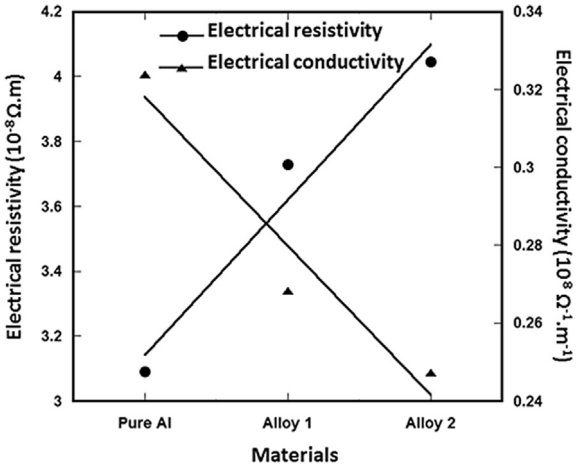

Fig. 7. Electrical conductivity and resistivity of pure Al, alloy 1 and alloy 2.

form a mixed crystal. Therefore, the electrons have difficulty moving from atom to atom in this new distorted structure. Thus, the resistance of the alloy becomes greater [23].

This reduction in electrical conductivity was intensified by increasing Mg content in alloy 2 due to the formation of intermetallic phase of Mg_2Si (electrical conductivity of $Mg_2Si = 14 \times 10^2\ \Omega^{-1}m^{-1}$) [24].

Fig. 8 show the electrical resistivity and conductivity of Si_3N_4 and coated silica fabricated composites.

Results of the ANOVA for electrical resistivity of the composites values are shown in Table 5. From Table 5 it can be understood that the relative portion of all the factors affect the electrical resistivity of the composites are almost in the same level. The percent contribution due to the error term in this analysis is 7%.

Considering the parameters included in Table 6 in the ranges tested, the maximum electrical resistivity value can be obtained by using the process parameters shown in Table 6. By using these process parameters, the projected electrical resistivity is 1.14×10^{-3} (Ω m) which is favorably consistent with verification value of 1.37×10^{-3} (Ω m).

This difference in electrical resistivity of composites could be related to the formation of new phases during infiltration process [25]. AlN ceramics with high electrical resistance (> 10^{12} Ω m) are considered as promising materials in electronic devices [26]. As explained, the amount of AlN phase in the final fabricated composite is controlled by different parameters, such as Mg concentration of alloy, time, temperature and atmosphere of infiltration process, etc. In the XRD pattern of L2-Al/Si_3N_4 composite, it can be observed the intensity peaks of AlN are stronger than those of silica coated composites. Therefore, high electrical resistivity of L2-Al/Si_3N_4 composite could be attributed to the formation of high amount of AlN during processing. Since, in silica coated composites, AlN phase in addition to the secondary phases of MgO and $MgAl_2O_4$ is formed, their electrical properties can affect the final properties of composite positively or negatively. $MgAl_2O_4$ exhibits much lower electric resistivity (0.83×10^{-2} Ω m) in comparison to AlN (> 10^{12} Ω m) [27]. Formation of $MgAl_2O_4$ is highly dependent on Mg concentration of alloy and can be decreased by reduction in Mg content of alloy. Another factor that influences the electrical resistivity of composite can be the volume fraction porosity. For composites with 40% volume fraction porosity, it is obvious that the electrical resistivity is higher than that for composites containing 60% one, because of more amount of non-conducting particulate reinforcements. According to the work of Vogelsang [28] reinforcement with particle size particularly below 10 μm strongly reduces the electrical conductivity of composite. By reducing a reinforcement size, the total stress and dislocation density as well as the radius of the deformation region increase drastically that negatively affect electrical conductivity.

3.5. Thermomechanical analysis

Fig. 9 depicts thermal strain response graph obtained while doing four cycles of heating and cooling processes between 25 °C and 250 °C on pure Al, alloy 1 and 2. Since, it is quite difficult to assess the thermal stress instead, thermal strain response curves are used to examine the thermal-cycling stability of the sample exposed to the harsh temperature changes. As we know, thermal stress results from thermal expansion inconsistency in materials while changing the temperature [29]. This stress can induce the thermal strain in the samples during thermal cycling. Such a thermal stress stems from uneven distribution of temperature in a sample, thermomechanical mismatch and thermal expansion anisotropy between two and single-phase materials, respectively [29,30]. The expansion and contraction of the samples with variation in the temperature clearly can be observed in Fig. 9. Thermal

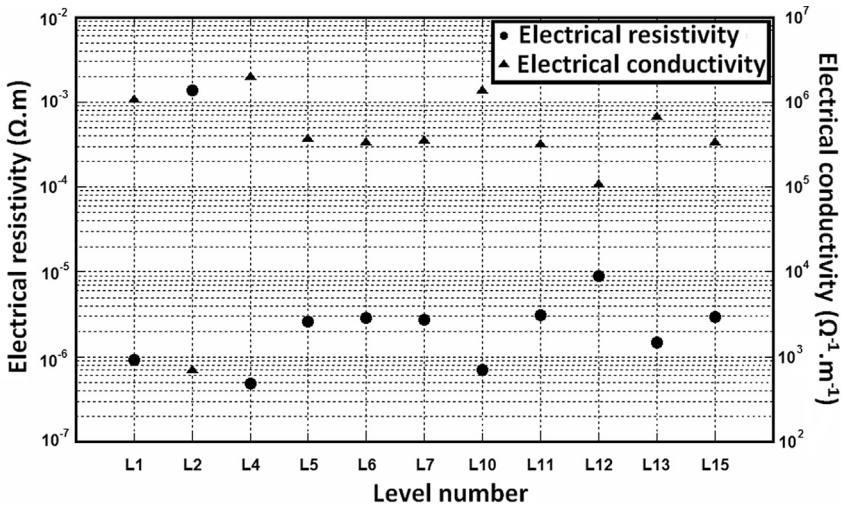

Fig. 8. Electrical conductivity and resistivity of Al/Si_3N_4 and Al/coated silica fabricated composites.

Table 5
Pooled ANOVA table for electrical resistivity (Ω m).

Column	Factors	Sum of squares	Variance	Contribution percentage
1	Alloy × Atmosphere	1.998 E−07	1.998 E−07	12
2	Porosity	2.01 E−07	2.01 E−07	12
3	Temperature × Time	2.61 E−07	2.61 E−07	15
4	Alloy	1.994 E−07	1.994 E−07	12
5	Atmosphere	1.29 E−07	1.29 E−07	8
6	Coating	2.62 E−07	2.62 E−07	15
7	Time	2 E−07	2 E−07	12
8	Temperature	1.24 E−07	1.24 E−07	7
Error		1.2 E−07		7
Total		1.7 E−06		100

Table 6
Optimal process parameters for maximum electrical resistivity (Ω.m).

Parameters	Proposed levels
Temperature (°C)	1200
Time (min)	120
Porosity (%)	40
Alloy	Low Mg
Atmosphere	N_2
Substrate	Si_3N_4

Table 7
Thermal response parameters and CTE of pure Al and Al-Mg-Si alloys with different content of Mg.

Materials	ε^p (10^{-4})	$\Delta\varepsilon^t$ (10^{-4})	ε^c (10^{-4})	CTE (10^{-6}/°C)
Pure Al	0.8744	5.5342	3.0857	28.17
Alloy 1	0.6838	3.0666	5.1578	25.29
Alloy 2	0.6164	2.8462	4.8252	24.07

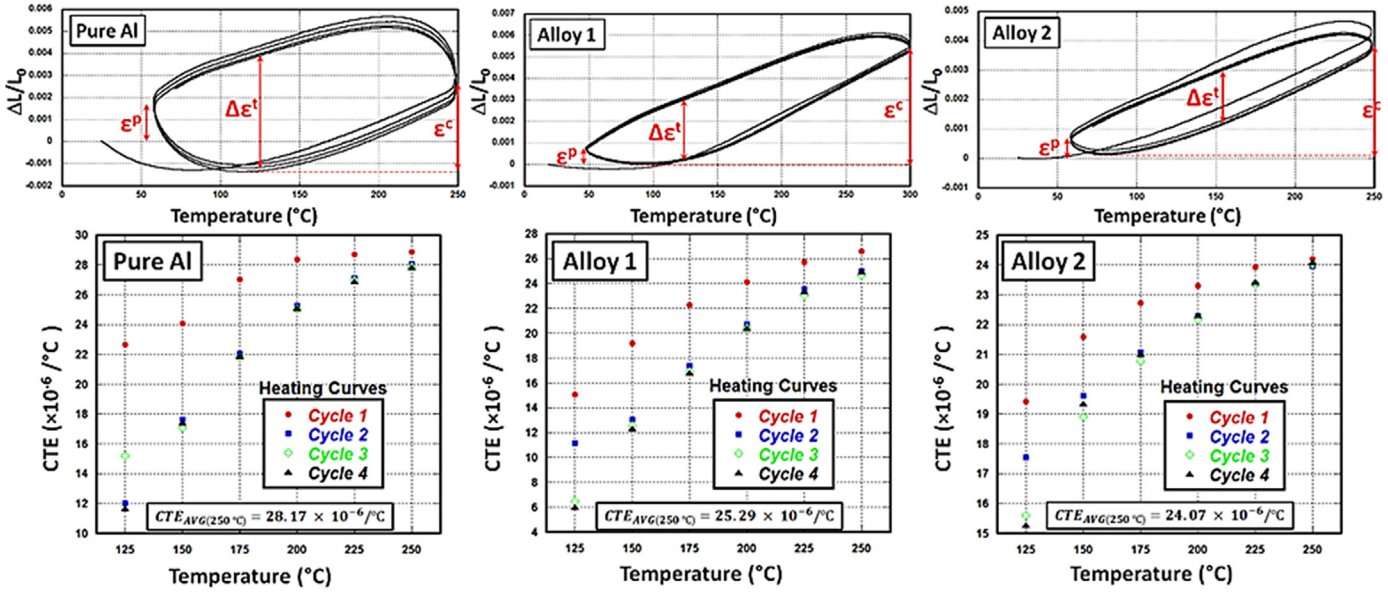

Fig. 9. Thermal strain response curve and CTE values obtained during the four cycles of heating and cooling between 25 °C and 250 °C on pure Al, alloy 1 and 2.

strain response graph showed more intensive thermal cycling in the first cycle and less intensive thermomechanical behavior for the subsequent thermal cycles.

Three parameters commonly utilized to characterize these curves are shown also in Fig. 9. The ε^p is used to determine the residual plastic strain, $\Delta\varepsilon^t$ is used to determine the largest vertical (at a given temperature) difference between the cooling and heating curves, and ε^c is the cyclic strain which gives information equivalent to that provided by the CTE. The degree of thermal damage and stability can be evaluated from ε^p, $\Delta\varepsilon^t$ and ε^c.

The thermal response outcomes of all samples from the heating of the first cycle to the cooling of the forth cycle is presented in Table 7. The results show that the $\Delta\varepsilon^t$ of all samples decreased as the percentage of alloying elements increased, representing that Si and Mg as well as Al is useful for the dimensional stability of Al-Mg-Si alloy.

Measured CTE of samples showed, their values can be strongly altered by thermal cycling. As it can be seen in Fig. 10, alloying leads to a reduction in the CTE value of pure Al. Greater amount of Mg in Alloy 2 increases the percentage of Mg_2Si intermetallic (CTE: 7.5×10^{-6}) in the alloy and consequently, more decline in CTE value of alloy 2 would be expected in comparison to alloy 1. The major difference between the coefficients of thermal expansion of the Al and the Mg_2Si/Si particles induces stresses and increases the dislocation density in the metal. As a result, the metal is hardened up to a degree. Basically, the higher the Mg_2Si content, the greater the metal hardness [29].

CTE values obtained from thermal strain response curves of all

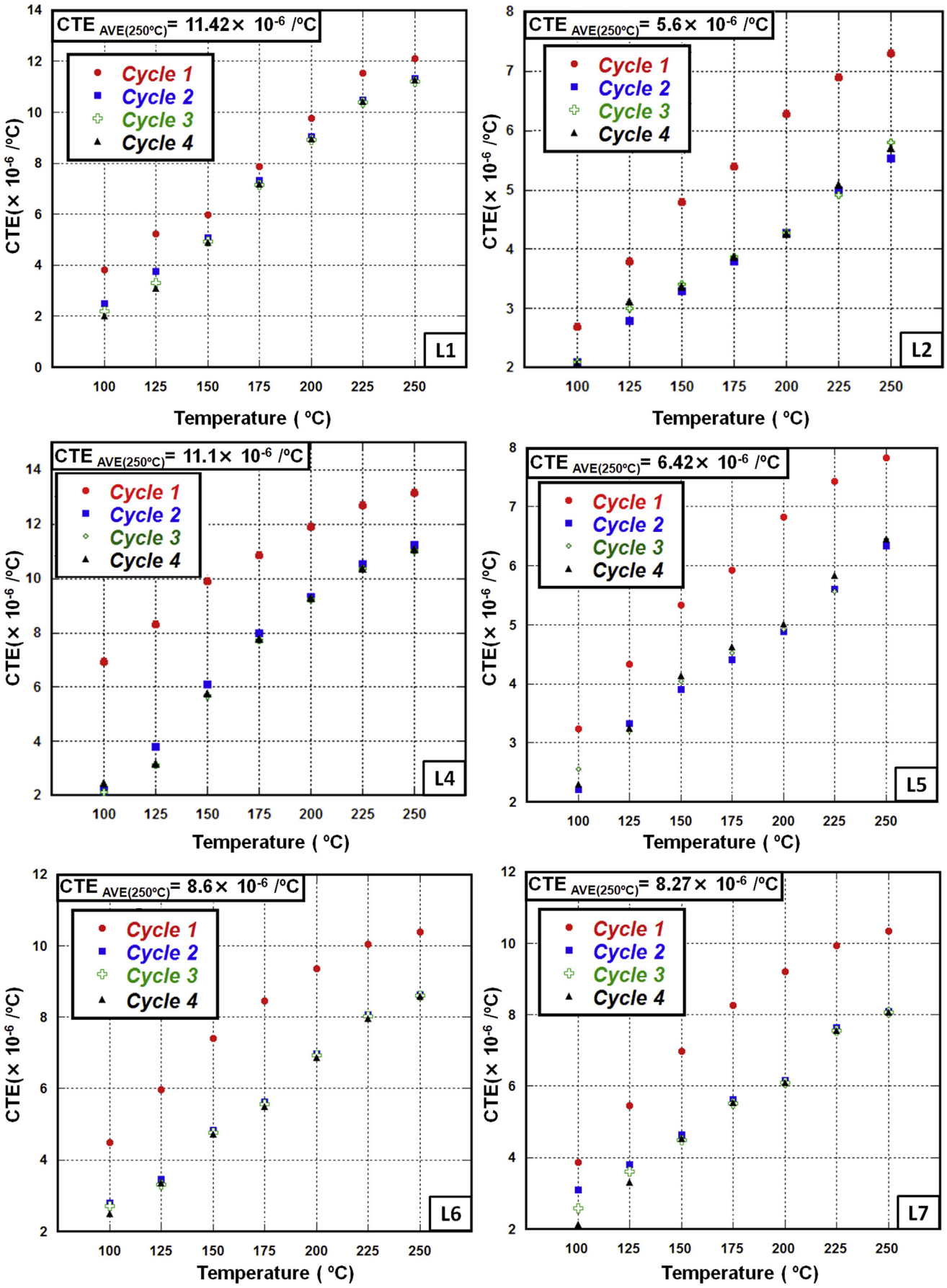

Fig. 10. CTE values calculated from heating curves of thermal strain response curve of fabricated composites, obtained during the four cycles of heating and cooling.

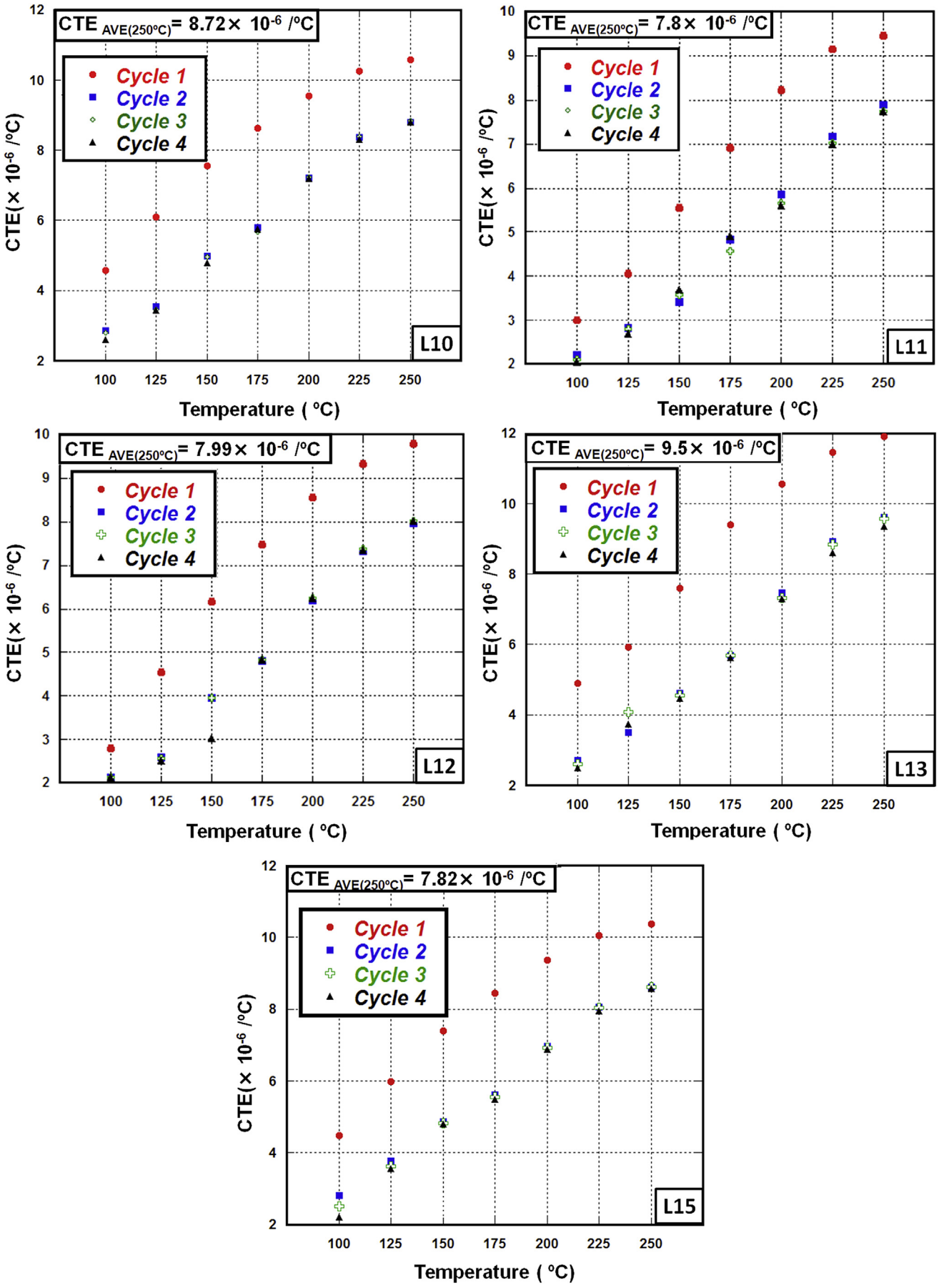

Fig. 10. (*continued*).

fabricated Si_3N_4 and coated silica composites are outlined in Fig. 10. In the matter of MMCs, thermal stress is understood to generate from the variance of the CTE values between the metal matrix and ceramic reinforcement phase. It is evident that excess reinforcing phase to Al-Si-Mg alloys leads to a drastic decrease in the value of CTE. Thermal hysteresis behavior can be explained in terms of the weak interface between reinforcements and matrix. Once the composite had been exposed to significant plastic deformation during the heating process due to exceed of thermal stresses beyond the yield strength of the matrix, large enough compressive stress could not be generated to alter the matrix form back to its initial size, while cooling, due to the lack of appropriate bonding force. Therefore, exceeded thermal stress in relation to the obtained stress of composite can cause the generation of strain hysteresis between the heating and cooling cycles.

As can be found in Fig. 10 at the beginning of the measurements, composites expanded at a low rate owning to the existence of residual thermal stresses in the samples. As the temperature increases, the thermal stress exerts as a tensile stress on the matrix. This thermal deformation of matrix enlarges the atom distance in the first cycle. As it can be seen during the subsequent heating cycles the tensioned matrix expands at a lower rate than the unstrained one does according to aggrandized atom distance (asymmetric curvature of potential energy) [30–32]. The thermal response results of all fabricated composites are shown in Table 8.

Outcomes of the pooled ANOVA for the CTE values are shown in Table 9. It indicates that, at the levels studied, the parameter that most significantly affects the CTE of the composites is porosity. Its relative contribution to the variance in composite density is 52%. It is evident that, the CTE varies with particle volume fraction. The CTEs of composites decrease as the content of reinforcements increases due to the constraint effect provided by the ceramic reinforcements with low CTEs. In other words, the higher the content of reinforcements, the larger the dislocation density and the larger the residual thermal stresses. Temperature of infiltration process also has a significant effect on CTE value of the composite, contributing 31% of the variance. It can be easy to notice that higher infiltration temperature leads to lower tendency to have uninfiltrated zones along the composite. Good bonding between matrix and reinforcement due to the proper temperature makes the major thermal expansion of composite being contributed by reinforcement. Therefore, the CTE of composites approach the reinforcing particle. The coating, atmosphere and Alloy × Atmosphere interaction also have minor effects on the CTE with relative contributions of 7, 6 and 2%, respectively. The thermal expansion behavior of composite is thermal history dependent. Thus, the CTE data should also depend on the thermal expansion behavior of Al-Si-Mg alloy. However, ANOVA analysis represents that the composition of Al does not have a major effect on CTE of the composites. This behavior could be due to the similarity of CTE values of these two alloys. The percent contribution because of the error term in this analysis is 2%.

Referring to the parameters existent in Table 9, in the range tested, the minimum CTE value can be obtained by using the process parameters shown in Table 10. When using these process parameters, the projected CTE is 4.44×10^{-6} (/°C) which compare to the verification value of 5.3×10^{-6} (/°C) is favorably concurred.

Generally speaking, processing conditions like temperature and time influence the microstructural features in the infiltration technique, especially the void content [33]. Increment in the infiltration time and temperature especially in presence of nitrogen improves the infiltration by formation of AlN and $MgAl_2O_4$ that consequently ameliorate the wettability of system and decreases the entrapped air voids [34]. However, the lower lattice mismatch of $MgAl_2O_4$ (0.25%) in comparison to AlN phase (8.7%) with Al suggests the strong interfacial bonding between matrix and $MgAl_2O_4$ reinforcement that eventually causes lower CTE value of composite fabricated by Si_3N_4 coated silica preform than those fabricated from Si_3N_4 preform [35,36].

3.6. Thermal diffusivity

Thermal diffusivity is a thermophysical property of a material and its value is directly proportional to the speed of propagation of heat in a medium by conduction when the temperature changes

Table 8
The thermal response results of all fabricated composites.

Composites	ε^p (10^{-4})	$\Delta\varepsilon^t$ (10^{-4})	ε^c (10^{-4})	*CTE* (10^{-6}/°C)
L1	0.8991	1.9421	2.66	11.42
L2	0.6835	0.7214	1.52	5.6
L4	0.8620	1.9342	2.41	11.1
L5	0.7212	1.3932	1.7	6.42
L6	0.7146	1.4173	2.17	8.6
L7	0.8748	1.3099	2.10	8.27
L10	0.8253	1.4120	2.21	8.72
L11	0.7985	1.0644	1.83	7.8
L12	0.8118	1.4039	1.98	7.99
L13	0.9713	1.5906	2.30	9.5
L15	0.7201	1.2591	1.84	7.82

Table 10
Optimal process parameters for minimum coefficient of thermal expansion (/°C).

Parameters	Proposed levels
Temperature (°C)	1200
Time (min)	120
Porosity (%)	40
Alloy	Low Mg
Atmosphere	N_2
Substrate	Si_3N_4 coated silica

Table 9
Pooled ANOVA table for coefficient of thermal expansion (/°C).

Column	Factors	Sum of squares	Variance	Contribution percentage
1	Alloy × Atmosphere	5.5 E−06	5.5 E−06	2
2	Porosity	1.4 E−04	1.4 E−04	52
3	Temperature × Time	Pooled	Pooled	–
4	Alloy	Pooled	Pooled	–
5	Atmosphere	1.6 E−05	11.6 E−05	6
6	Coating	1.8 E−05	1.8 E−05	7
7	Time	Pooled	Pooled	–
8	Temperature	8.1 E−05	8.1 E−05	31
Error		5.2 E−06	1.7 E−06	2
Total		2.6 E−04		100

with time. The relationship between thermal diffusivity α (m^2/s), specific heat C_p (J/kg K), thermal conductivity λ (W/m K), and density ρ (kg/m^3) can be given by the following equation [37]:

$$\propto = \frac{\lambda}{\rho C_p} \tag{6}$$

Fig. 11 depicts the thermal diffusivity of the pure Al and two utilized alloys in this investigation. As it can be found, thermal diffusivity of pure Al decreases while increasing the temperature. However, the thermal diffusivity of two alloys showed lower thermal diffusivity values and less dependent on temperature in comparison to that for pure Al. Owning to large contribution of electrons in thermal conduction, metals are considered as an extremely good conductor of heat. By alloying a metal the efficiency of electron motions to conduct a heat is decreasing. Alloying elements can act a scattering center and improves the phonon-phonon scattering and significantly reduces the thermal diffusivity.

Due to the approximately linear relationship between thermal diffusivity and electrical conductivity based on Wiedemann-Franz Law [38], in this study two samples from higher and two samples from lower value of electrical conductivity out of all fabricated composites have been selected. Four samples under condition of L2, L4, L10 and L12 have been selected based on electrical results. As it

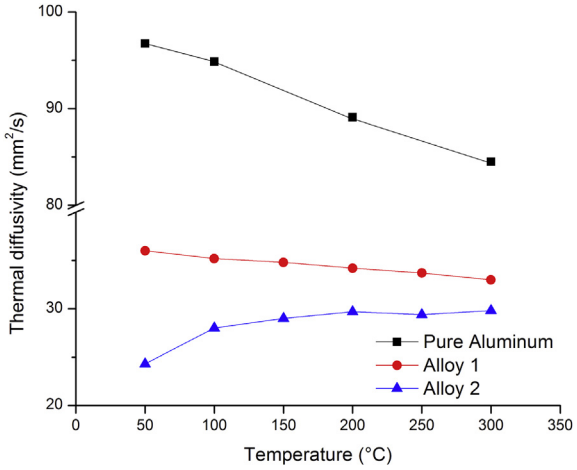

Fig. 11. Thermal diffusivity of pure Al [47,48], alloy 1 and 2 at different temperatures.

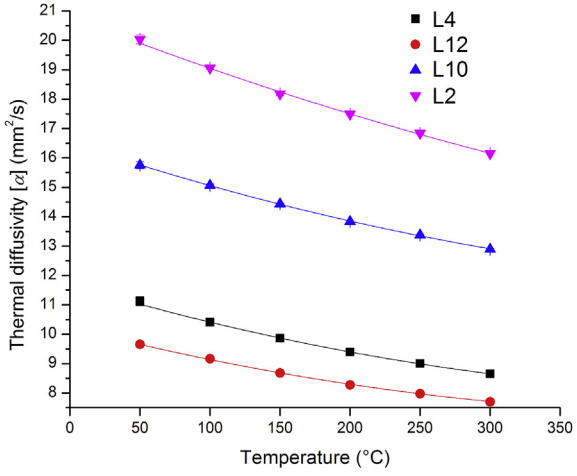

Fig. 12. Thermal diffusivity of fabricated composite at different temperatures.

can be seen in Fig. 12 at 50 °C the maximum and minimum thermal diffusivity values of 20.4 and 9.8 mm^2/s have been achieved under condition of L2 and L12, respectively. Although the fabricated sample under L2 condition exhibits lower electrical conductivity than that under condition of L10, it showed better performance in thermal diffusivity. As has been seen in all composite samples, thermal diffusivity decreases with increasing temperature. It shows various parameters such as holding temperature, holding time, content of magnesium in Al alloy, type of atmosphere influences making high thermal diffusivity composite.

Lower thermal diffusivity of studied ceramics particles such as silicon dioxide (0.0083 cm^2/s), AlN (0.8 cm^2/s), $MgAl_2O_4$ (0.15 cm^2/s) and Si_3N_4 (0.12 cm^2/s) [39,40] at room temperature in comparison to that value for pure Al shows the phonons are not as effective as electron in transport of heat energy as a result of phonon scatterings by lattice imperfections. Also, these reduction could be due to interfacial barrier like oxidation of reinforcement, fiber coating and differences in coefficient thermal expansion between reinforcement and matrix [41].

One of the reason that the prepared sample under L2 condition showed a relatively good thermal diffusivity can be due to its high amount of AlN. However, despite being well-known that AlN has a high thermal diffusivity but its structure was found to be very sensitive to an oxygen and Mg content. Because, oxygen impurities and diffusion of Mg atoms into the AlN produce mass defects of Al vacancies, which leads to enhancement of phonon scattering. It has been reported that thermal diffusivity of AlN can increases from 1.5 to 12 mm^2/s with the decrease in oxygen concentration from 13.6 to 1.1 at.% [42,43]. In addition, the particle size and morphology of AlN phase can affect its thermal diffusivity. Coarser and more oriented AlN needles in direction of heat flow can increase thermal diffusivity of the composite [44]. It has been reported that the phases formed by VLS mechanism has the highest thermal diffusivity value [45]. The other factor that made AlN phase less effective in the fabricated composite can be related to its lattice mismatch of 8.7% than that of 0.25% for $MgAl_2O_4$ with Al. This mismatch may cause internal stress which can lead to microcracking of component or interfacial separation that results in major decrease in thermal diffusivity [46]. Under condition of L4 and L12 because of $MgAl_2O_4$ formation from silica and its good adhesion to Al matrix, the thermal diffusivity of the composites improved, the lattice mismatch of AlN and Al have been reduced by growth of AlN onto $MgAl_2O_4$ in samples prepared by Si_3N_4 coated silica. $MgAl_2O_4$ and AlN films have an in-plane lattice mismatch of 6.4% [43]. However, L2 and L10 samples prepared by Si_3N_4 preforms showed higher values than those under L4 and L12. These variances could be due to the inherent higher thermal diffusivity value of AlN than that for $MgAl_2O_4$.

4. Conclusions

5) Lack of spontaneous infiltration of Al alloys into SiO_2 preform has been improved by Si_3N_4 coating. Formation of AlN in all the fabricated composites shows this phase plays a vital role in pressureless infiltration process of Si_3N_4 and Si_3N_4 coated silica preforms. Formation of MgO and $MgAl_2O_4$ were just observed in coated silica preforms. MgO exists besides $MgAl_2O_4$ at higher Mg content alloy.
6) At the levels studied for pressureless infiltration of fabricated composites, the parameter that most significantly affects the modulus of elasticity is process temperature following by atmosphere.
7) The maximum modulus of elasticity can be obtained by using tempreture (1200 °C), time (120 min), porosity of 40 vol%,

alloy (low Mg), under atmosphere of N_2 and Si_3N_4 preform are 265 GPa.

8) At the levels studied for pressureless infiltration of fabricated composites, the parameter that most significantly affects the CTE value is porosity content of preform.
9) The minimum value of CTE can be obtained by using tempreture (1200 °C), time (120 min), porosity of 40 vol%, alloy (low Mg), under atmosphere of N_2 and Si_3N_4 coated silica preform is 5.3×10^{-6} (/°C).
10) At the levels studied for pressureless infiltration of fabricated composites, the parameter that most significantly affects the electrical resistivity/conductivity is coating of preform.
11) The maximum value of electrical resistivity can be obtained by using tempreture (1200 °C), time (120 min), porosity of 40 vol%, alloy (low Mg), under atmosphere of N_2 and Si_3N_4 preform is 5.3×10^{-6} (/°C).
12) The projected values for modulus of elasticity, porosity content,, CTE value and electrical resistivity of fabricated composite through ANOVA are in an excellent agreement to those obtained from test which carried on according the factors proposed by ANOVA.
13) Thermal diffusivity of all fabricated samples were measured. The results show that fabricated composite under L2 has a higher value of 20.4 mm^2/s in comparison to other fabricated levels.

Acknowledgment

Mr. Amin Bahrami and Ms. Niloofar Soltani gratefully acknowledge Conacyt (National Council of Science and Technology, in Mexico) for granting a doctoral scholarship. The authors are also thankful to Cinvestav IPN-Saltillo for support in the research activities in the field of advanced materials.

References

[1] V. Nardone, K. Prewo, On the strength of discontinuous silicon carbide reinforced aluminum composites, Scr. Metall. 20 (1986) 43–48.
[2] J. Torralba, C. Da Costa, F. Velasco, P/M aluminum matrix composites: an overview, J. Mater. Process. Technol. 133 (2003) 203–206.
[3] N. Soltani, A. Bahrami, M.I. Pech-Canul, The effect of Ti on mechanical properties of extruded in-situ Al-15 pct Mg_2Si composite, Metall. Mater. Trans. A 44 (2013) 4366–4373.
[4] N. Soltani, M.I. Pech-Canul, A. Bahrami, Effect of 10Ce-TZP/Al_2O_3 nanocomposite particle amount and sintering temperature on the microstructure and mechanical properties of Al/(10Ce-TZP/Al_2O_3) nanocomposites, Mater. Des. 50 (2013) 85–91.
[5] A.D. Moghadam, E. Omrani, P.L. Menezes, P.K. Rohatgi, Mechanical and tribological properties of self-lubricating metal matrix nanocomposites reinforced by carbon nanotubes (CNTs) and graphene–a review, Compos. Part B Eng. 77 (2015) 402–420.
[6] R. Deaquino-Lara, N. Soltani, A. Bahrami, E. Gutiérrez-Castañeda, E. García-Sánchez, M. Hernandez-Rodríguez, Tribological characterization of Al7075–graphite composites fabricated by mechanical alloying and hot extrusion, Mater. Des. 67 (2015) 224–231.
[7] N. Nasiri, M. Emamy, A. Malekan, M. Norouzi, Microstructure and tensile properties of cast Al–15% Mg_2Si composite: effects of phosphorous addition and heat treatment, Mater. Sci. Eng. A 556 (2012) 446–453.
[8] N. Nasiri, M. Emamy, A. Malekan, Microstructural evolution and tensile properties of the in situ Al–15% Mg_2Si composite with extra Si contents, Mater. Des. 37 (2012) 215–222.
[9] N. Sobczak, R. Asthana, W. Radziwill, R. Nowak, A. Kudyba, The role of aluminium oxidation in the wetting-bonding relationship of Al oxide couples, Arch. Metall. Mater. 52 (2007) 55.
[10] M. Emamy, M. Khodadadi, A.H. Raouf, N. Nasiri, The influence of Ni addition and hot-extrusion on the microstructure and tensile properties of Al–15% Mg_2Si composite, Mater. Des. 46 (2013) 381–390.
[11] A. Bahrami, M.I. Pech-Canul, C. Gutierrez, N. Soltani, Effect of rice-husk ash on properties of laminated and functionally graded Al/SiC composites by one-step pressureless infiltration, J. Alloys Compd. 644 (2015) 256–266.
[12] A. Bahrami, M.I. Pech-Canul, C. Gutiérrez, N. Soltani, Wetting and reaction characteristics of crystalline and amorphous SiO_2 derived rice-husk ash and SiO_2/SiC substrates with Al–Si–Mg alloys, Appl. Surf. Sci. 357 (2015) 1104–1113.
[13] P. Rohatgi, R. Guo, H. Iksan, E. Borchelt, R. Asthana, Pressure infiltration technique for synthesis of aluminum–fly ash particulate composite, Mater. Sci. Eng. A 244 (1998) 22–30.
[14] W. Shouren, G. Haoran, Z. Jingchun, W. Yingzi, Interpenetrating microstructure and properties of Si_3N_4/Al–Mg composites fabricated by pressureless infiltration, Appl. Compos. Mater. 13 (2006) 115–126.
[15] A. Bahrami, U. Simon, N. Soltani, S. Zavareh, J. Schmidt, M.I. Pech-Canul, A. Gurlo, Eco-fabrication of hierarchical porous silica monoliths by ice- templating of rice husk ash, Green Chem. (2016), http://dx.doi.org/10.1039/c6gc02153k.
[16] N. Soltani, A. Bahrami, M.I. Pech-Canul, L. González, Review on the physicochemical treatments of rice husk for production of advanced materials, Chem. Eng. J. 264 (2015) 899–935.
[17] A. Bahrami, N. Soltani, M.I. Pech-Canul, C. Gutiérrez, Development of metal-matrix composites from industrial/agricultural waste materials and their derivatives, Crit. Rev. Environ. Sci. Technol. 46 (2016) 143–208.
[18] A. Leal-Cruz, Synthesis and Characterization of Silicon Nitride Reinforcements by the Thermal Decomposition of Na_2SiF_6 in Nitrogen Containing Atmosphere, M. Sc. thesis, Cinvestav Saltillo. Saltillo Coah., México, 2004.
[19] F.M. Smits, Measurement of sheet resistivities with the four-point probe, Bell Syst. Tech. J. 37 (1958) 711–718.
[20] V.M. Sreekumar, R. Pillai, B. Pai, M. Chakraborty, Evolution of $MgAl_2O_4$ crystals in Al-Mg-SiO_2 composites, Appl. Phys. A 90 (2008) 745–752.
[21] X. Ning, T. Okamoto, Y. Miyamoto, A. Koreeda, K. Suganuma, Reaction chemistry at joined interfaces between silicon nitride and aluminium, J. Mater. Sci. 26 (1991) 4142–4149.
[22] J. Achenbach, Wave Propagation in Elastic Solids, Elsevier, 2012.
[23] W.W. Hintalla, The Electrical Conductivity of the Copper-aluminum Alloys, 1937.
[24] J.-i. Tani, H. Kido, Thermoelectric properties of Sb-doped Mg_2Si semiconductors, Intermetallics 15 (2007) 1202–1207.
[25] H. Nasery, M. Medraj, M.D. Pugh, Processing and Characterization of Aln-mgo-mgal2o4 Composites by Spontaneous Infiltration, University of Concordia, Montreal, Canada, pp. 389–399.
[26] Y.W. Leung, AlN Thick Films for Power Electronic Device Applications, MSc thesis, Hong Kong University of Science and Technology, 1999.
[27] S. Angappan, L.J. Berchmans, C. Augustin, Sintering behaviour of $MgAl_2O_4$—a prospective anode material, Mater. Lett. 58 (2004) 2283–2289.
[28] M. Vogelsang, R.J. Arsenault, R.M. Fisher, An in situ HVEM study of dislocation generation at Al/SiC interfaces in metal matrix composites, Metall. Trans. A 17 (1986) 379–389.
[29] C.H. Hsueh, P.F. Becher, Thermal stresses due to thermal expansion anisotropy in materials with preferred orientation, J. Mater. Sci. Lett. 10 (1991) 1165–1167.
[30] M.A. Dellis, J.P. Keustermans, F. Delannay, J. Wegria, Zn-Al matrix composites: investigation of the thermal expansion, creep resistance and fracture toughness, Mater. Sci. Eng. A 135 (1991) 253–257.
[31] S.Q. Wu, Z.S. Wei, S.C. Tjong, The mechanical and thermal expansion behavior of an Al–Si alloy composite reinforced with potassium titanate whisker, Compos. Sci. Technol. 60 (2000) 2873–2880.
[32] S.-Y. Chang, S.-J. Lin, M.C. Flemings, Thermal expansion behavior of silver matrix composites, Metall. Mater. Trans. A 31 (2000) 291–298.
[33] M. Kobashi, M. H., N. K., SiC/aluminum composites fabricated by in situ processing using reactive infiltration aid, in: 12th International Conference on Aluminium Alloys, Yokohama, Japan, 2010, pp. 1886–1890.
[34] N.Y. Taranets, Y.V. Naidich, Wettability of aluminum nitride by molten metals, Powder Metall. Metal Ceram. 35 (1996) 282–285.
[35] Y. Zhou, Z. Yu, N. Zhao, C. Shi, E. Liu, X. Du, C. He, Microstructure and properties of in situ generated $MgAl_2O_4$ spinel whisker reinforced aluminum matrix composites, Mater. Des. 46 (2013) 724–730.
[36] W. Wang, H. Qian, W. Yang, H. Wang, Y. Zhu, G. Li, Effect of Al substrate nitridation on the properties of AlN films grown by pulsed laser deposition and its mechanism, J. Alloys Compd. 644 (2015) 444–449.
[37] Y.S. Touloukian, R. Powell, C. Ho, M. Nicolaou, Thermophysical Properties of Matter-the TPRC Data Series, vol. 10, 1974. Thermal Diffusivity, in, DTIC Document.
[38] M.J. Graf, S.K. Yip, J.A. Sauls, D. Rainer, Electronic thermal conductivity and the Wiedemann-Franz law for unconventional superconductors, Phys. Rev. B 53 (1996) 15147–15161.
[39] R. Haubner, M. Herrmann, B. Lux, G. Petzow, R. Weissenbacher, M. Wilhelm, M. Jansen, High Performance Non-oxide Ceramics II, Springer, 2003.
[40] B. Schulz, Thermophysical properties of sapphire, AlN and $MgAl_2O_4$ down to 70 K, J. Nucl. Mater. 212 (1994) 1065–1068.
[41] S. Somiya, Handbook of Advanced Ceramics: Materials, Applications, Processing, and Properties, Academic Press, 2013.
[42] T. Yagi, N. Oka, T. Okabe, N. Taketoshi, T. Baba, Y. Shigesato, Effect of oxygen impurities on thermal diffusivity of AlN thin films deposited by reactive RF magnetron sputtering, Jpn. J. Appl. Phys. 50 (2011) 11RB01.
[43] G. Li, J. Ohta, A. Kobayashi, H. Fujioka, Room-temperature epitaxial growth of AlN on atomically flat MgAl2O4 substrates, Appl. Phys. Lett. 89 (2006) 2104.
[44] D. Hasselman, K.Y. Donaldson, A.L. Geiger, Effect of reinforcement particle size on the thermal conductivity of a particulate-silicon carbide-reinforced aluminum matrix composite, J. Am. Ceram. Soc. 75 (1992) 3137–3140.
[45] R. Quinn, Thermal Diffusivity and Conductivity in Ceramic Matrix Fiber Composite Materials-literature Study, Lockheed Martin Corporation,

Schenectady, NY 12301 (US), 2000.
[46] B.R. Powell, G. Youngblood, D. Hasselman, L.D. Bentsen, Effect of thermal expansion mismatch on the thermal diffusivity of Glass-Ni composites, J. Am. Ceram. Soc. 63 (1980) 581–586.
[47] J.E. Hatch, A. Association, Aluminum: Properties and Physical Metallurgy, ASM International, 1984.
[48] E.H. Buyco, F.E. Davis, Specific heat of aluminum from zero to its melting temperature and beyond. Equation for representation of the specific heat of solids, J. Chem. Eng. Data 15 (1970) 518–523.